Title
The need for higher-order averaging in the stability analysis of hovering, flapping-wing flight

Journal
Bioinspiration & Biomimetics, 10(1)

ISSN
1748-3182

Authors
Taha, Haithem E
Tahmasian, Sevak
Woolsey, Craig A
et al.

Publication Date
2015

DOI
10.1088/1748-3190/10/1/016002

Peer reviewed

The need for higher-order averaging in the stability analysis of hovering, flapping-wing flight

2015 Bioinspir. Biomim. 10 016002

(http://iopscience.iop.org/1748-3190/10/1/016002)

Bioinspiration & Biomimetics

CrossMark

RECEIVED
21 July 2014

ACCEPTED FOR PUBLICATION
16 November 2014

PUBLISHED
5 January 2015

PAPER

The need for higher-order averaging in the stability analysis of hovering, flapping-wing flight

Haithem E Taha[1], **Sevak Tahmasian**[2], **Craig A Woolsey**[2], **Ali H Nayfeh**[2] **and Muhammad R Hajj**[2]

[1] University of California, Irvine, CA, USA
[2] Virginia Polytechnic Institute and State University, Blacksburg, VA, USA

E-mail: hetaha@uci.edu

Keywords: flapping flight, insect hovering stability, higher order averaging, nonlinear, time-periodic systems, flight dynamics

Abstract

Because of the relatively high flapping frequency associated with hovering insects and flapping wing micro-air vehicles (FWMAVs), dynamic stability analysis typically involves direct averaging of the time-periodic dynamics over a flapping cycle. However, direct application of the averaging theorem may lead to false conclusions about the dynamics and stability of hovering insects and FWMAVs. Higher-order averaging techniques may be needed to understand the dynamics of flapping wing flight and to analyze its stability. We use second-order averaging to analyze the hovering dynamics of five insects in response to high-amplitude, high-frequency, periodic wing motion. We discuss the applicability of direct averaging versus second-order averaging for these insects.

1. Introduction

Flapping flight dynamics has long been a topic of interest to researchers, particularly following the studies of Taylor and Thomas [1] among others. Even simple models of flapping flight dynamics involve multi-body, nonlinear, non-autonomous (time-varying) dynamics. One common assumption used in flapping flight dynamic models is that the effect of the wing inertial forces on the body dynamics may be neglected [2–10]. The validity of this assumption is a subject of continuing debate; see the recent review of Taha *et al* [11] or Sun [12]. Nevertheless, researchers usually adopt this assumption because (i) the mass of the wing is very small with respect to that of the body and (ii) ignoring the multi-body effects yields equations of motion similar to those governing the flight dynamics of conventional aircraft. However, there remains a major distinction between the dynamics of flapping flight and that of a conventional aircraft. Because of the time-varying aerodynamic loads due to the wing oscillatory motion, the flapping flight dynamic model is time-varying.

By neglecting wing inertial effects, the flight dynamics of a flapping-wing micro-air-vehicle (FWMAV) can be represented by a nonlinear, time-periodic (NLTP) system. Stability analysis for such systems is usually performed using one of the two approaches schematically presented in figure 1. In the first approach, one uses averaging to obtain a nonlinear, time-invariant (NLTI) system model. For high enough flapping frequency, the averaging theorem guarantees that exponential stability of a fixed point for the NLTI model implies exponential stability of the corresponding periodic orbit of the NLTP system. To determine exponential stability of the fixed point, one may simply linearize the NLTI system to obtain a linear, time-invariant (LTI) model and examine the eigenvalues of the state matrix for the LTI system. This first approach has been adopted in a variety of early studies, with varying degrees of formality and rigor [2–4, 6–9, 13–15].

A less common approach, adopted by Dietl and Garcia [5] and Bierling and Patil [16], and later by Weihua and Cesnik [17], involves solving numerically for the periodic solution that corresponds to hovering motion in the original NLTP system. Linearizing about this periodic orbit yields a linear, time-periodic (LTP) system whose stability can be analyzed using the Floquet theorem. Specifically, one solves for the fundamental response of the LTP system over a single period to obtain the monodromy matrix; that is, the state transition matrix evaluated at the fundamental period. Stability analysis involves checking the eigenvalues of this monodromy matrix.

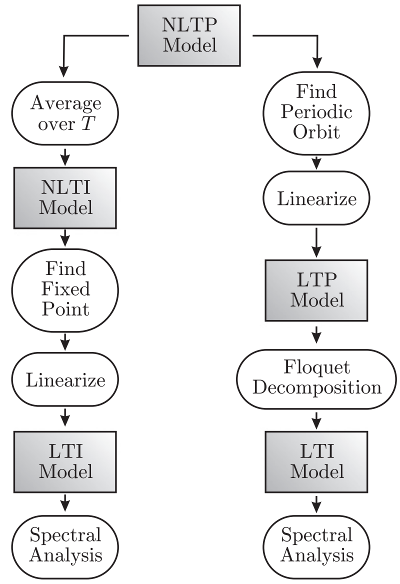

Figure 1. Two approaches to analyze the stability of nonlinear, time-periodic systems.

Hovering usually involves relatively high flapping frequencies, compared to forward flight; flapping frequencies of hovering insects typically fall within the range of 20–1000 Hz [18]. The dynamics of hovering insects exhibits two time scales: a fast time scale for the variation of the aerodynamic loads and a slow time scale for the aggregate motion of the body. For example, while a flying insect's general motion is perceptible to a human's eye, the flapping motion of its wings may not be. If the ratio of the two time scales is large enough, then averaging may be intuitively justifiable and, hence, provides a tractable approach for the stability analysis. A notable advantage of the averaging approach is that one need not obtain a solution for the hovering flight condition in advance; one can instead solve for fixed points of the time-averaged system with the expectation that these fixed points correspond to periodic orbits in the original system. One great advantage of the second approach involving Floquet analysis is that it does not require a large separation of time scales for the flapping and aggregate motions. However, this approach does require finding the periodic orbit in advance. Moreover, application of the Floquet theorem requires obtaining the fundamental matrix solution for an LTP system which can be a practical challenge, even if it is formally straight forward. Finding the periodic motion and solving for the fundamental matrix solution must typically be done numerically. In summary, although the Floquet theorem approach does not have limitations on the structure and the nature of the time-periodic system under study, its inevitable numerical implementation precludes scrutinizing the dynamical behavior of the system on an analytical level. On the other hand, although the averaging approach allows for analytical treatment of the problem, its limitation to large separation between the system's time-scales makes its application to the dynamics of hovering insects/ FWMAVs with relatively low flapping frequencies (e.g., hawkmoth) questionable.

In an earlier work [19], we used the method of multiple scales (MMS) [20, 21] to determine a second-order approximate solution to the hovering dynamic equations of insects and FWMAVs and demonstrated the shortcomings of direct averaging. In this work, we consider an extension of the averaging approach that relaxes the requirement for a large separation of time scales with the objective to analytically study the flight dynamics and stability of hovering insects and FWMAVs. This extension was presented by Sarychev [22] and Vela [23], applying the concepts of exponential representation of flows and the chronological calculus proposed by Agrachev and Gamkrelidze [24]. Sarychev [22] and Vela [23] provided a generalization of the averaging theorem to cases where the system is not weakly forced or the ratio of time scales is not very large. They provided algorithmic procedures for averaging a system's dynamic model to an arbitrarily high-order. Thus, if first-order (direct) averaging is not sufficiently accurate, because the system is subjected to high-amplitude, periodic forcing or because the two time scales are not widely separated, one may use second-order, or third-order averaging, etc. In this work, we provide some examples that illustrate the limitations of direct averaging. Then, we use second-order averaging to analyze the flight dynamics of several hovering insects and, hence, assess the region of applicability of direct averaging.

2. Flight dynamic model

For the relatively large insects of concern to this study and the common FWMAVs, the wing mass is negligible with respect to the body mass (less than 5%), the effect of the wing inertial forces are neglected. As such, the body dynamics is described by the same set of equations as a conventional, rigid aircraft. We focus on longitudinal flight dynamics and use the standard body-fixed reference frame [25] to formulate the flight dynamic equations. Given a reference point, such as the center of mass, to serve as the origin, we let x_b denote the longitudinal axis; that is, the axis which is aligned with the fuselage in a conventional aircraft. We let y_b denote the lateral axis, pointing in the direction of the starboard wingtip, and we let z_b complete the orthogonal triad. We define a vector of longitudinal state variables $\boldsymbol{x} = [u, w, q, \theta]^T$, where u and w are the components of the body's inertial velocity along the x_b and z_b directions, respectively. The angle θ is the pitch angle about the y_b-axis and q is the pitch rate. Figure 2 shows a schematic diagram for a FWMAV whose wing sweeps forward and backward in a horizontal plane and pitches about a chord line to vary the wing's angle of attack during the stroke. The

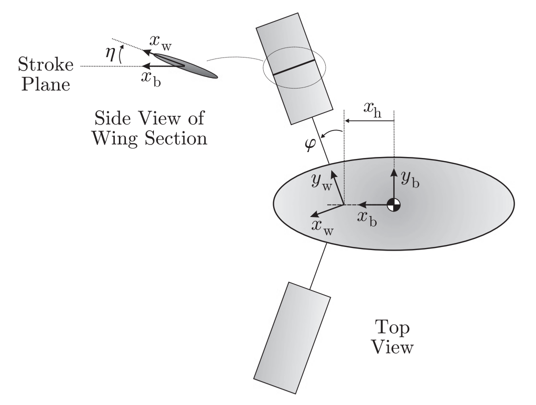

Figure 2. Schematic diagram for a hovering FWMAV whose wing sweeps in a horizontal stroke plane where φ is the back-and-forth flapping angle and η is the wing pitching angle.

wing's axis system x_W-y_W-z_W is obtained from the body's axis system x_b-y_b-z_b by translating a distance x_h along the x_b-axis, rotating by an angle $-\varphi$ about the z_b-axis and then by an angle η about the y_W-axis.

2.1. Kinematics and morphology

Otherwise stated, a triangular waveform for the back and forth flapping angle $\varphi(t)$ and a piecewise constant variation for the pitching angle $\eta(t)$, which maintains a constant angle of attack α_m throughout the entire stroke, are used in this work; that is,

$$\varphi(t) = \begin{cases} \dfrac{4\Phi}{T}\left(t - \dfrac{T}{4}\right), & 0 \leqslant t < \dfrac{T}{2} \\ -\dfrac{4\Phi}{T}\left(t - \dfrac{3T}{4}\right), & \dfrac{T}{2} \leqslant t < T \end{cases} \quad \text{and}$$
$$\eta(t) = \begin{cases} \alpha_m, & 0 \leqslant t < \dfrac{T}{2}, \\ \pi - \alpha_m, & \dfrac{T}{2} \leqslant t < T. \end{cases} \tag{1}$$

The choice of this kinematics is based on the result that this combination of $\varphi(t)$ and $\eta(t)$ yields hovering with minimum aerodynamic power [26]. The wing planform and the morphological parameters of the hawkmoth as well as the other insects under study are given in appendix A.

2.2. Aerodynamic–dynamic interaction

Written explicitly, the longitudinal equations are

$$\begin{pmatrix} \dot{u} \\ \dot{w} \\ \dot{q} \\ \dot{\theta} \end{pmatrix} = \begin{pmatrix} -qw - g\sin\theta \\ qu + g\cos\theta \\ 0 \\ q \end{pmatrix} + \begin{pmatrix} \dfrac{1}{m}X(\boldsymbol{x}, t) \\ \dfrac{1}{m}Z(\boldsymbol{x}, t) \\ \dfrac{1}{I_y}M(\boldsymbol{x}, t) \\ 0 \end{pmatrix}, \tag{2}$$

where g is the gravitational acceleration, m and I_y represent the body mass and the pitch inertia, respectively. The generalized forces X and Z are the aerodynamic forces in the x_b- and z_b-directions, respectively, and M is the aerodynamic moment about the y_b-axis. Recognizing that the aerodynamic forces and moment will depend explicitly on time for a FWMAV, equation (2) can be written in the more general form

$$\dot{\boldsymbol{x}} = \boldsymbol{f}(\boldsymbol{x}) + \boldsymbol{g}_a(\boldsymbol{x}, t). \tag{3}$$

The flight dynamic model used in this paper was developed in an earlier work [27]. Here, we neglect higher-order dependence of the non-autonomous aerodynamic vector field $\boldsymbol{g}_a$ on the state vector $\boldsymbol{x}$ and retain only the linear terms to obtain

$$\begin{pmatrix} \dot{u} \\ \dot{w} \\ \dot{q} \\ \dot{\theta} \end{pmatrix} = \begin{pmatrix} -qw - g\sin\theta \\ qu + g\cos\theta \\ 0 \\ q \end{pmatrix} + \begin{pmatrix} \dfrac{1}{m}X_0(t) \\ \dfrac{1}{m}Z_0(t) \\ \dfrac{1}{I_y}M_0(t) \\ 0 \end{pmatrix}$$
$$+ \begin{bmatrix} X_u(t) & X_w(t) & X_q(t) & 0 \\ Z_u(t) & Z_w(t) & Z_q(t) & 0 \\ M_u(t) & M_w(t) & M_q(t) & 0 \\ 0 & 0 & 0 & 0 \end{bmatrix} \begin{pmatrix} u \\ w \\ q \\ \theta \end{pmatrix}. \tag{4}$$

Assuming a horizontal stroke plane, parameterized by the 'back-and-forth' flapping angle φ, and a piecewise constant variation in the wing pitch angle η, one obtains [27]

$$X_0(t) = -2K_{21}\dot{\varphi}(t)\left|\dot{\varphi}(t)\right| \cos\varphi(t)\sin^2\eta,$$
$$Z_0(t) = -K_{21}\dot{\varphi}(t)\left|\dot{\varphi}(t)\right| \sin 2\eta,$$

$$M_0(t) = 2\dot{\varphi}(t)\left|\dot{\varphi}(t)\right| \sin\eta\Big[K_{22}\Delta\hat{x}\cos\varphi(t)$$
$$+ K_{21}x_h\cos\eta(t) + K_{31}\sin\varphi(t)\cos\eta\Big],$$

where x_h is the distance from the vehicle center of mass to the root of the wing hinge line (i.e., the intersection of the hinge line with the x_b-axis) and $\Delta\hat{x}$ is the chordwise distance from the center of pressure to this same hinge location, normalized by the chord length. Also, ρ is the air density, C_{L_α} is the three-dimensional lift curve slope of the wing, $c(r)$ is the spanwise chord distribution, R is the wing radius, $I_{mn} = 2\int_0^R r^m c^n(r)\,\mathrm{d}r$, and $K_{mn} = \frac{1}{4}\rho C_{L_\alpha} I_{mn}$. The time-varying stability derivatives are written directly in terms of the system parameters as [27]

$$X_u = -4\frac{K_{11}}{m}\left|\dot{\varphi}\right| \cos^2\varphi\sin^2\eta,$$
$$X_w = -\frac{K_{11}}{m}\left|\dot{\varphi}\right| \cos\varphi\sin 2\eta,$$
$$X_q = \frac{K_{21}}{m}\left|\dot{\varphi}\right| \sin\varphi\cos\varphi\sin 2\eta - x_h X_w,$$

$$Z_u = 2X_w,$$
$$Z_w = -2\frac{K_{11}}{m}\left|\dot{\varphi}\right|\cos^2\eta,$$
$$Z_q = 2\frac{K_{21}}{m}\left|\dot{\varphi}\right|\sin\varphi\cos^2\eta - \frac{K_{\mathrm{rot}_{12}}}{m}\dot{\varphi}\cos\varphi - x_h Z_w,$$
$$M_u = 4\frac{K_{12}\Delta x}{I_y}\left|\dot{\varphi}\right|\cos^2\varphi\sin\eta + \frac{m}{I_y}\left(2X_q - x_h Z_u\right),$$
$$M_w = 2\frac{K_{12}\Delta x}{I_y}\left|\dot{\varphi}\right|\cos\varphi\cos\eta + 2\frac{K_{21}}{I_y}\left|\dot{\varphi}\right|\sin\varphi\cos^2\eta - \frac{mx_h}{I_y}Zw,$$
$$M_q = -\frac{2\Delta x}{I_y}\left|\dot{\varphi}\right|\cos\varphi\cos\eta\left(K_{12}x_h + K_{22}\sin\varphi\right) + \frac{1}{I_y}\dot{\varphi}\cos\varphi\left(K_{\mathrm{rot}_{13}}\Delta x\cos\varphi\cos\eta + K_{\mathrm{rot}_{22}}\sin\varphi\right) - \frac{2}{I_y}\left|\dot{\varphi}\right|\cos^2\eta\sin\varphi \times\left(K_{21}x_h + K_{31}\sin\varphi\right) - \frac{K_v\mu_1 f}{I_y}\cos^2\varphi - \frac{mx_h}{I_y}Z_q,$$

where $K_{\mathrm{rot}_{mn}} = \pi\rho\left(\frac{1}{2} - \Delta\hat{x}\right)I_{mn}$ and $K_v = \frac{\pi}{16}\rho I_{04}$. The hinge line is set at 30%c ($\Delta\hat{x} = 0.05$) and the value of C_{L_α} is calculated based on the wing aspect ratio using the extended lifting theory according to Taha *et al* [28, 29]. The above flight dynamic model has been developed in [27] and the resulting eigenvalues of the averaged, linearized dynamics have been validated against numerical simulations of Navier–Stokes equations by Sun *et al* [15] and the experimental data of Cheng and Deng [30]. These details are omitted for conciseness of this work.

3. Issues with previous approaches

In [19], we showed that direct application of the averaging theorem (i.e., first-order averaging) does not capture the true stability characteristics of the hovering hawkmoth. We supported this claim by performing direct integration of the system under study and by applying the Floquet theorem approach. We summarize these results here for the completeness of this paper. In this section, we also show that careless choices of the numerical integrator and its time-step for the implementation of the Floquet theorem approach may also lead to false conclusions about the system's stability.

3.1. Direct averaging approach

A finite-dimensional, non-autonomous dynamical system is represented by

$$\dot{x} = \epsilon Y(x, t). \tag{5}$$

If Y is T-periodic in t, the averaged dynamical system corresponding to equation (5) is written as

$$\dot{\bar{x}} = \epsilon\bar{Y}\left(\bar{x}\right), \tag{6}$$

where $\bar{Y}(x) = \frac{1}{T}\int_0^T Y(x, \tau)\mathrm{d}\tau$. According to the averaging theorem (see Khalil [31] for example), if ϵ is small enough, then exponential stability of a fixed point of the averaged system implies exponential stability of the corresponding periodic orbit of the original time-periodic system.

Following [2, 27, 32], we scale the time variable in equation (3) as $\tau = \frac{\omega}{\omega_n}t$, where ω is the flapping frequency and ω_n is the natural frequency of the body motion. As such, for a large enough $\frac{\omega}{\omega_n}$, the dynamics in the new time variable is of the form (5) with $\epsilon \equiv \frac{\omega_n}{\omega}$ (i.e., amenable to the averaging theorem). It should be noted that, for hovering insects of the lowest flapping frequency (hawkmoth), the ratio $\frac{\omega}{\omega_n}$ is as high as 30, which has usually been used as a justification of direct averaging. Then, the averaged dynamics of equation (3) is written as [27]

$$\dot{\bar{x}} = f\left(\bar{x}\right) + \bar{g}_a\left(\bar{x}\right), \tag{7}$$

where $\bar{x}$ is the averaged state vector and $\bar{g}_a(\bar{x})$ is the average of the vector field $g_a(x, t)$ over the flapping period; that is, $\bar{g}_a(x) = \frac{1}{T}\int_0^T g_a(x, \tau)\mathrm{d}\tau$.

A main advantage of the averaging approach is its extremely easy trim procedure in comparison to the Floquet theorem approach. Suppose the flapping motion is characterized by a vector of parameters $\boldsymbol{P}$ (e.g., flapping frequency, stroke amplitude and feathering angle) and denote this parametric dependence as follows: $g_a(x, t; \boldsymbol{P})$ and $\bar{g}_a(\bar{x}; \boldsymbol{P})$. If balance/trim at hover is required, the trim problem is stated as follows: determine the flapping parameters $\boldsymbol{P}$ that are necessary to ensure $f(\mathbf{0}) + \bar{g}_a(\mathbf{0}; \boldsymbol{P}) = \mathbf{0}$. This is achieved by solving a set of algebraic equations. In contrast, the trim problem using the Floquet theorem approach is stated as follows: determine the flapping parameters $\boldsymbol{P}$ and the periodic orbit $x^*(t)$ such that

$$\dot{x}^*(t) = f\left(x^*(t)\right) + g_a\left(x^*(t), t; \boldsymbol{P}\right)$$

with $\bar{x}^* = \mathbf{0}$. Obviously, it is a much harder problem and often cannot be solved analytically. It requires a double iteration loop, where the inner loop is used to capture a periodic orbit corresponding to some set of flapping parameters, and the outer loop is used to iterate on $\boldsymbol{P}$ to obtain a periodic orbit with zero mean (for hovering).

Adopting the averaging approach to achieve balance/trim at hover yields the well-known conditions

$$\bar{X}_0 = 0, \quad -\bar{Z}_0 = \bar{L}_0 = mg, \quad \bar{M}_0 = 0,$$

where $\bar{L}_0$ is the cycle-averaged lift force due to flapping. This trim approach leads to the known

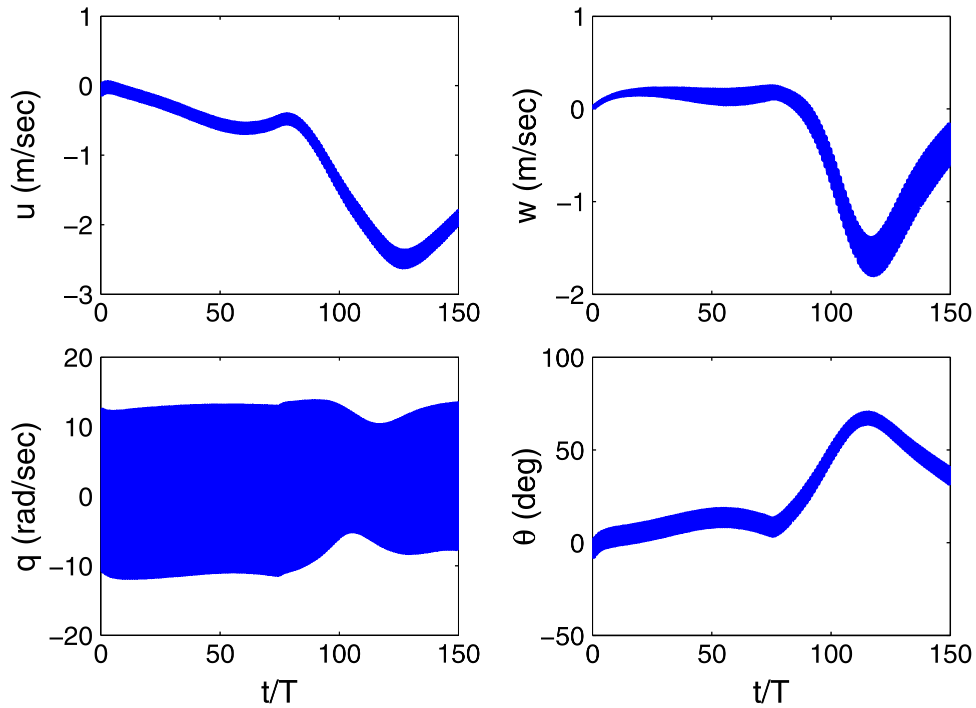

Figure 3. Simulation of the nonlinear flight dynamics (4) of the hovering hawkmoth.

intuitive conclusion that symmetric back and forth flapping automatically ensures zero cycle-averaged forward thrust force. In addition, aligning the hinge line to coincide with the vehicle's center of mass ($x_h = 0$) ensures pitch trim ($\overline{M}_0 = 0$.) Then, the hovering vehicle has to flap enough to support its weight. This dictates a certain combination of flapping amplitude Φ, frequency $f = \frac{1}{T}$, and mean angle of attack α_m. Having ensured trim at hover (such that the origin is a fixed point for the averaged system), the stability of this equilibrium may be investigated. By the statement of the averaging theorem, exponential stability of this fixed point yields exponential stability of the hovering periodic orbit for the original time-varying system. A necessary and sufficient condition for local exponential stability of the origin of equation (7) is that the Jacobian of its vector field evaluated at the origin be Hurwitz.

For the hawkmoth case, the resulting eigenvalues of the averaged, linearized system matrix are

$$0.19 \pm 5.74\text{i}, \quad -11.89, \quad -3.30$$

which indicates an unstable system. This approach has been adopted in [3, 4, 13–15, 27, 30, 33, 34] to assess the stability of flapping dynamics. Similar to the obtained results, almost all of the previous studies concluded instability for hovering flight. Deceptively, simulating the original system (4) supports this conclusion, as shown in figure 3. The states of the system do not oscillate about zero means, but rather deviate from the hovering equilibrium. However, this deviation from the equilibrium is not really due to the predicted instability; a deeper look into the dynamics is required. To show that, we consider the following example.

To obtain equation (4) from equation (2), the aerodynamic vector field $\boldsymbol{g}_a$ is written as

$$\boldsymbol{g}_a(\boldsymbol{x}, t) = \boldsymbol{g}_0(t) + [\boldsymbol{G}(t)]\boldsymbol{x},$$

where $\boldsymbol{g}_0$ represents the aerodynamic loads due to the flapping motion of the wing and the matrix $\boldsymbol{G}$ represents the time-varying stability derivatives (i.e., the aerodynamic loads due to body motion). The periodic terms $\boldsymbol{g}_0$ and $\boldsymbol{G}$ can be written as

$$\boldsymbol{g}_0(t) = \overline{\boldsymbol{g}_0} + \boldsymbol{g}_1(t), \qquad \boldsymbol{G}(t) = \overline{\boldsymbol{G}} + \boldsymbol{G}_1(t),$$

where $\overline{\boldsymbol{g}_0}$ and $\overline{\boldsymbol{G}}$ are the cycle-averaged components of $\boldsymbol{g}_0$ and $\boldsymbol{G}$, respectively, while $\boldsymbol{g}_1$ and $\boldsymbol{G}_1$ are the corresponding zero-mean components, which vanish under the direct application of the averaging theorem. Because $\boldsymbol{g}_1$ and $\boldsymbol{G}_1$ are of zero-mean, stability analysis using direct averaging yields the same result irrespective of their inclusion. Consider the following system, in which we omit $\boldsymbol{g}_1$ but retain $\boldsymbol{G}_1$ to assess the role of the time-varying nature of the stability derivatives:

$$\dot{\chi} = \boldsymbol{f}(\chi) + \overline{\boldsymbol{g}_0} + \left[\overline{\boldsymbol{G}} + \boldsymbol{G}_1(t)\right]\chi. \qquad (8)$$

The system (8) has a fixed point at the origin at all times because the above trim procedure (based on direct averaging) yields $\boldsymbol{f}(\boldsymbol{0}) + \overline{\boldsymbol{g}_0} = \boldsymbol{0}$. Moreover, the averaged, linearized version of this system has the exact same eigenvalues as the original system presented in equation (4); that is, direct application of the averaging theorem concludes instability for the system (8) as well. However, many simulations such as the

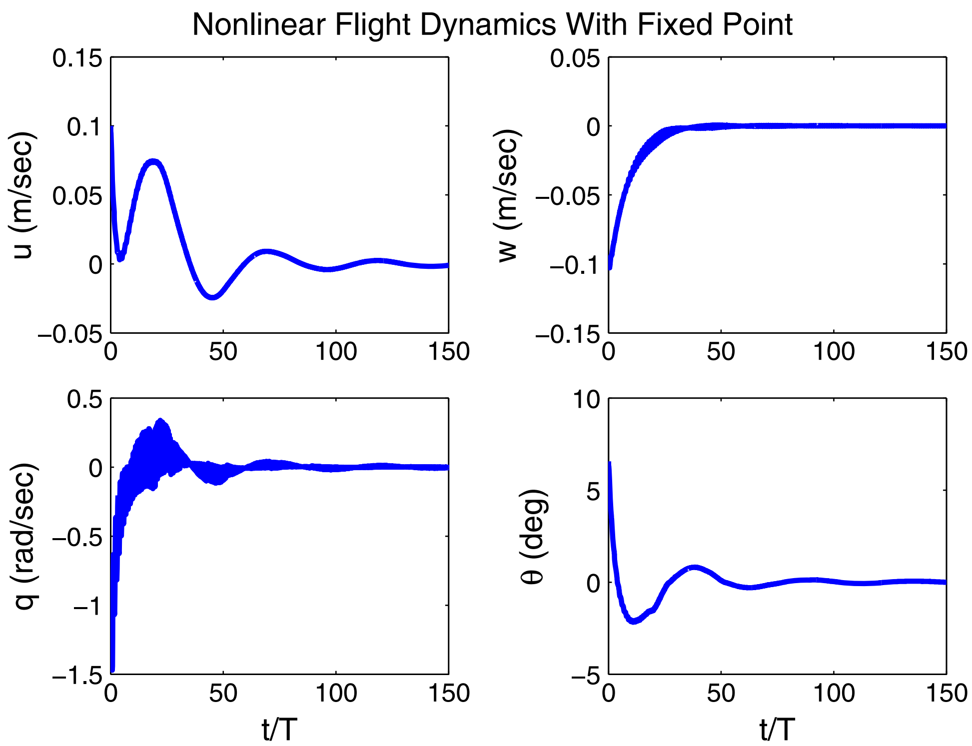

Figure 4. Simulation of the nonlinear flight dynamics, omitting the periodic external forcing, equation (8).

one shown in figure 4 indicate that the system (8) is stable.

Figure 4 shows that direct application of the averaging theorem is not sufficient to analyze the stability of the system (8). It should be noted that the time-invariant systems obtained through direct averaging of (8) and the original hovering flight dynamics (4) are the same. Hence, the instability deduced from the simulation shown in figure 3 is not attributed to the averaging analysis. In addition, figure 4 shows that the high-frequency periodic signals of the hovering dynamics (represented by G_1) may provide stabilizing actions, as indicated in an earlier work [19]. In fact, this is a well-known characteristic of high-frequency, high-amplitude, periodic forcing, known as vibrational stabilization (see Bullo [35] and Sarychev [22], for example), or stabilization via parametric excitation (see Nayfeh and Mook [36]).

3.2. Floquet theorem approach

To further support the simulation results of the system (8) shown in figure 4, we apply the Floquet theorem. Unlike the system (4), the system (8) has a fixed point representing the equilibrium not a periodic orbit. So, the step of finding the periodic orbit is skipped. Linearizing the system (8) about the origin, we obtain

$$\dot{\chi}(t) = \left[Df(\mathbf{0}) + \overline{G} + G_1(t) \right] \chi(t) \qquad (9)$$

which is a LTP system that is amenable to the Floquet theorem. Even in this relatively simple case, the Floquet theorem must be applied numerically. The system (9) is simulated using four independent initial conditions at $t = 0$ until $t = T$. These initial state vectors are stacked column-wise to form a square matrix $[IC]$. Similarly, the corresponding solutions at the period T are collected in a matrix $[\Xi]$. The monodromy matrix is then given by

$$[M] = [IC]^{-1}[\Xi].$$

The eigenvalues of M are called the Floquet multipliers. If all of the Floquet multipliers lie inside the unit circle, then the origin is an exponentially stable fixed point for the system (9) (see Nayfeh and Mook [36] and Nayfeh and Balachandran [37] for example), which implies exponential stability of the origin of the system (8) by Lyaponuv indirect method [31]. Using a traditional, fixed step (100 points per cycle), fourth-order Runge–Kutta integrator, the following Floquet multipliers are obtained:

$$0.96 \pm 0.11\mathrm{i}, \quad 0.6881, \quad 0.8889.$$

All of these eigenvalues lie inside the unit circle indicating stability of the system (8), supporting the simulation results, and refuting the direct averaging results.

It is interesting to note that careless choices of the integrator and its time step in the implementation of the Floquet theorem approach may lead to false conclusions about the system's stability. Using $[IC] = 0.1[II]$, where $[II]$ represents the identity matrix, and Matlab ode45 solver (adaptive step), the following Floquet multipliers are obtained

$$0.78 \pm 0.074i, \quad 1.0497, \quad 0.8887$$

which indicate an unstable system in spite of the stability of the system shown in figure 4 and concluded from the more careful Floquet analysis described earlier. In addition to the numerical errors that may arise due to careless choices of the solver and/or the integration time-step, implementing the Floquet theorem for a general NLTP, such as the one presented in equation (3), may induce errors due to the numerical determination of the periodic orbit and the linearization around this obtained periodic orbit. Viewing the Floquet approach as an exact (complete) averaging, it is interesting to present a deeper look on the commutativity of linearization and averaging in appendix B. Finally, the reader is referred to the work of Wu *et al* [38], which the authors deem one of the most complete work on insect flight dynamics employing the Floquet theorem approach.

4. The proposed approach: higher-order averaging

While direct averaging may be valid for weakly forced systems or very high-frequency forcing, the generalized averaging theory (GAT) can be applied successfully to high-amplitude, high-frequency, periodic forcing, because it provides an arbitrarily higher-order approximation to the flow along the time-periodic vector field. In addition, unlike the Floquet theorem approach, the GAT provides a compact way of analyzing NLTP systems. Thus, it can be used analytically and, hence, avoids any numerical errors. Furthermore, the analytical tractability of the GAT leads to a better understanding of the system dynamics, as shown below.

Agrachev and Gamkrelidze laid the foundation for the GAT in their seminal work [24]. A solution to the non-autonomous differential equation (5) with $\boldsymbol{x}(0) = \boldsymbol{x}_0$ can be written using the Volterra series expansion as

$$\boldsymbol{x}(t) = \boldsymbol{x}_0 + \sum_{m=1}^{\infty} \int_0^t \int_0^{\tau_1} \dots \times \int_0^{\tau_{m-1}} \mathcal{Y}(\boldsymbol{x}_0)\, \mathrm{d}\tau_m \dots \mathrm{d}\tau_1, \tag{10}$$

where

$$\mathcal{Y} = \left(Y_{\tau_1} \circ Y_{\tau_2} \circ \dots \circ Y_{\tau_m}\right).$$

Here, $Y_\tau(\boldsymbol{x}) = Y(\boldsymbol{x}, \tau)$ and $\circ$ denotes the composition of maps; that is, $\left(Y_{\tau_1} \circ Y_{\tau_2}\right)(\boldsymbol{x}) = Y_{\tau_1}(Y_{\tau_2}(\boldsymbol{x}))$. Agrachev and Gamkrelidze provided the conditions of convergence of the series presented in equation (10). Similar to the exponential representation of solutions to autonomous differential equations, Agrachev and Gamkrelidze denoted the flow of the non-autonomous vector field Y_τ as $\overrightarrow{\exp}\left(\int_0^t Y_\tau \mathrm{d}\tau\right)$ and called it the *chronological exponential*. They also defined the *logarithm* of this exponential map as

$$V_t = \ln \overrightarrow{\exp}\left(\int_0^t Y_\tau \mathrm{d}\tau\right).$$

That is, the flow along the autonomous vector field V_t for a unit time is equivalent to the flow along the non-autonomous vector field Y_τ for a time t. Although V_t is an autonomous vector field, it is parametrized by time; that is, if the final time t is changed, the vector field will change. Agrachev and Gamkrelidze have shown that $V_t = \sum_{m=1}^{\infty} V_t^{(m)}$, where

$$V_t^{(m)} = \int_0^t \int_0^{\tau_1} \dots \int_0^{\tau_{m-1}} \mathcal{G}_m\left(Y_{\tau_1}, \dots, Y_{\tau_m}\right) \mathrm{d}\tau_m \dots \mathrm{d}\tau_1$$

and $\mathcal{G}_m$ are commutator polynomials. The first three polynomials are written as

$$\mathcal{G}_1(\zeta_1) = \zeta_1, \quad \mathcal{G}_2(\zeta_1, \zeta_2) = \frac{1}{2}\left[\zeta_2, \zeta_1\right],$$

$$\mathcal{G}_3(\zeta_1, \zeta_2, \zeta_3) = \frac{1}{6}\left(\left[\zeta_3, \left[\zeta_2, \zeta_1\right]\right] + \left[\left[\zeta_3, \zeta_2\right], \zeta_1\right]\right),$$

where $[\cdot, \cdot]$ is the commutator which, for vector fields, is the Lie bracket. Thus, Agrachev and Gamkrelidze provided an algorithmic approach to analytically determine the logarithm of time-periodic vector fields.

Sarychev [22] and Vela [23] utilized the above concepts to develop a generalization for the classical averaging theorem. Sarychev [22] introduced the notion of *complete averaging* to denote the following averaged vector field corresponding to the time-periodic system (5):

$$\overline{Y} = \frac{1}{T} \ln \overrightarrow{\exp}\left(\int_0^T Y_\tau \mathrm{d}\tau\right) = \frac{1}{T} V_T. \tag{11}$$

Thus, one can write the averaged system corresponding to the NLTP system in (5) as

$$\dot{\overline{\boldsymbol{x}}} = \epsilon \overline{Y} = \epsilon \boldsymbol{\Lambda}_1(\overline{\boldsymbol{x}}) + \epsilon^2 \boldsymbol{\Lambda}_2(\overline{\boldsymbol{x}}) + \cdots, \tag{12}$$

where

$$\boldsymbol{\Lambda}_1(\overline{\boldsymbol{x}}) = \frac{1}{T} \int_0^T Y(\boldsymbol{x}, t)\, \mathrm{d}t,$$

$$\boldsymbol{\Lambda}_2(\overline{\boldsymbol{x}}) = \frac{1}{2T} \int_0^T \left[\int_0^t Y(\boldsymbol{x}, \tau)\, \mathrm{d}\tau, Y(\boldsymbol{x}, t)\right].$$

The power of the GAT lies in the fact that the $\boldsymbol{\Lambda}$'s can be computed analytically in terms of Lie brackets between the vector fields describing the time-periodic dynamics. Sarychev [22] and Vela [23] related this generalization of the averaging theorem to the nonlinear extension of the Floquet theorem and showed that the averaged vector field $\overline{Y}$ is the logarithm of the the Monodromy map in the nonlinear case: the nonlinear vector-valued function that maps an initial state to the solution at the fundamental period.

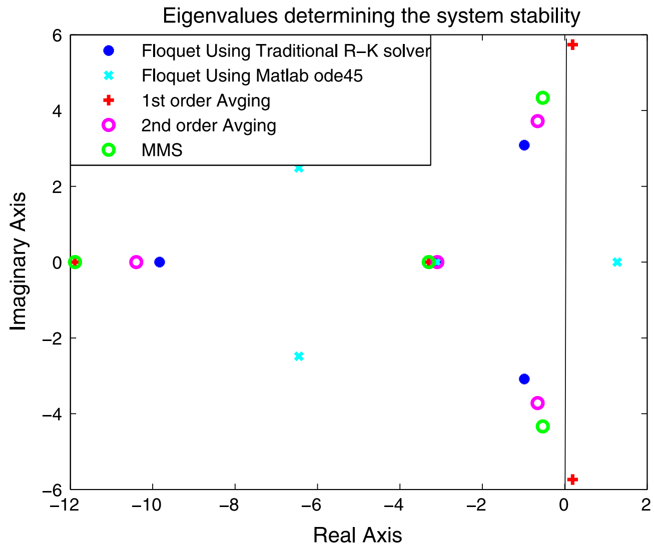

Figure 5. Eigenvalues determining the stability of the time-periodic system (8) for the hawkmoth case using first-order averaging, second-order averaging, method of multiple scales (MMS) [19], Floquet theorem with the traditional Runge–Kutta solver, and Floquet theorem using the Matlab ode45 solver.

4.1. Hovering dynamics omitting the periodic external forcing: fixed point equilibrium

In this subsection, we show that second-order averaging is able to more accurately capture the stability characteristics of the example considered in the last section (hovering dynamics with fixed point), which is presented in equation (8). Setting $f(\mathbf{0}) + \overline{g}_0 = \mathbf{0}$ ensures that the origin is a fixed point for the system (8) and all of its averaged dynamics (first, second, …). Having assured balance, it is sufficient to study the eigenvalues of the linearized, second-order averaged dynamics $D(\boldsymbol{\Lambda}_1 + \boldsymbol{\Lambda}_2)(\mathbf{0})$ which (for the hawkmoth case) are

$$-0.66 \pm 3.72\mathrm{i}, \quad -10.40, \quad -3.09.$$

These eigenvalues indicate that the system is stable. Figure 5 shows the resulting eigenvalues that determine the stability of the system (8) using first-order averaging, second-order averaging, MMS [19], Floquet theorem with the traditional Runge–Kutta solver, and Floquet theorem with Matlab ode45 solver. To have the same eigenvalue representation, the presented eigenvalues using the Floquet theorem approach are the Floquet multipliers transformed from the $\mathcal{Z}$-plane to the $\mathcal{S}$-plane via the common transformation $z = e^{Ts}$ [39].

Figure 5 shows that the stability characteristics using second-order averaging and the MMS better matches the results of a carefully implemented Floquet analysis in comparison to direct averaging and the Floquet theorem approach using the Matlab ode45 solver. One interesting note from figure 5 is that all of the approaches resulted in the same eigenvalue at −3.09 for the vertical motion. It should be noted that the vertical motion is decoupled from the forward and pitching motions near hover [15, 27]. Thus, the direct averaging can provide a good estimate for the eigenvalue corresponding to the vertical motion

$$\lambda_w = \overline{Z_w} = -8\frac{K_{11}\Phi}{mT}\cos^2\alpha_m$$

for constant angle of attack α_m with any $\varphi(t)$-waveform.

Figure 6 shows the simulations of the full nonlinear dynamics, with fixed point, in equation (8) along with the first and second-order averaged dynamics for the hawkmoth near hovering equilibrium. The w-motion is matched in the three simulations (note that w is decoupled from the other three degrees of freedom and its eigenvalue is well predicted by first-order averaging). However, the simulation of the first-order averaged dynamics (7) for the other three degrees of freedom $(u - q - \theta)$ diverges from both of the second-order averaged dynamics and full system simulations. The simulation of the first-order averaged dynamics show growing oscillations as may be expected, while the simulations of the NLTP system (8) as well as its second-order averaged dynamics show stable solutions.

4.2. Induced stabilizing mechanism

One of the interesting outcomes from the GAT is the ability to specifically determine the stabilizing mechanism induced by the high-frequency, high-amplitude, periodic terms. To show that, we consider the linearized, first-order averaged system-matrix for the hawkmoth case

$$D(\boldsymbol{\Lambda}_1)(\mathbf{0}) = \begin{bmatrix} -3.59 & 0 & 0 & -9.81 \\ 0 & -3.30 & 0 & 0 \\ 39.95 & 0 & -7.92 & 0 \\ 0 & 0 & 1 & 0 \end{bmatrix}.$$

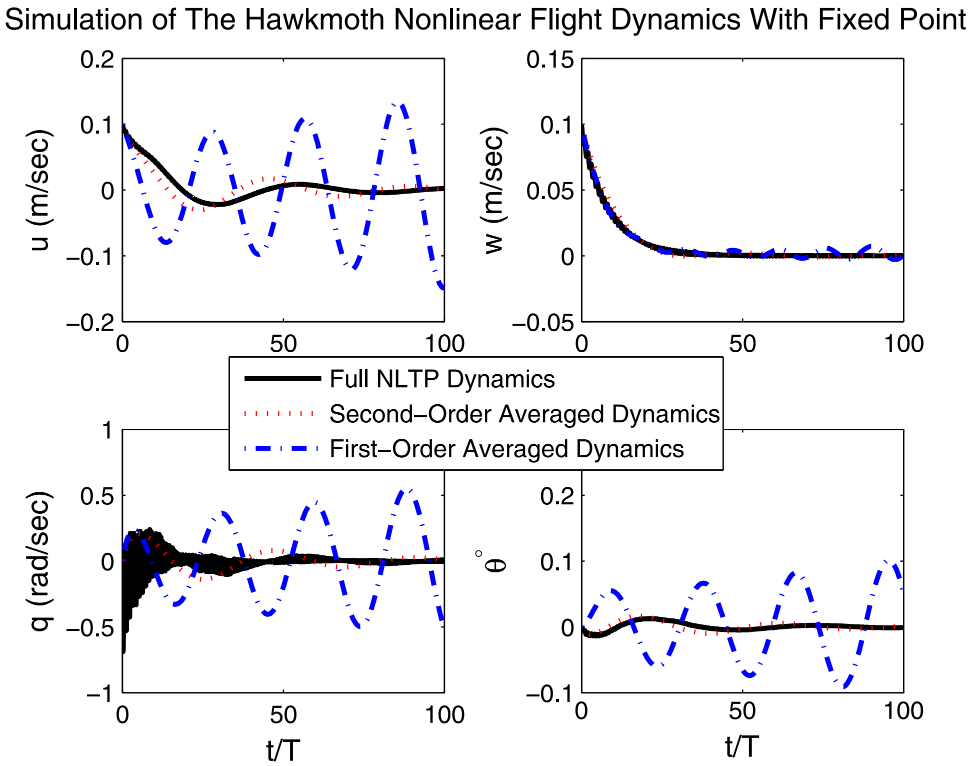

Figure 6. Simulation of the NLTP system (8) for the hawkmoth case in comparison to simulations of the first and second-order averaged dynamics.

Using the adopted trim procedure (symmetric flapping and zero x_h), the system lacks any pitch-stiffness [27]. There is no aerodynamic pitching moment M due to the body pitching angle θ in most of the flying vehicles. Moreover, the adopted trim procedure leads to zero M due to w (or α); the essential stability derivative for the static stability of conventional aircraft [25]. However, due to the high-amplitude, high-frequency, periodic forcing, the system gains a considerable pitch-stiffness that is shown in the (3, 4) element of the linearized, second-order averaged system-matrix

$$D\left(\boldsymbol{\Lambda}_1 + \boldsymbol{\Lambda}_2\right)(\mathbf{0}) = \begin{bmatrix} -3.58 & 0 & 0 & -9.81 \\ 0 & -3.09 & 0 & 0 \\ 29.98 & 0 & -8.13 & -28.45 \\ -2.90 & 0 & 0.96 & 0 \end{bmatrix}.$$

The periodic terms lead to a small reduction in the damping in the forward and vertical directions. It also leads to a reduction in the value of the speed stability (M due to u) which is a favorable effect [27]. On the other hand, the pitch damping becomes larger. Of particular interest is the generation of a considerable pitch stiffness (negative M due to θ). Thus, the GAT allows specifying the stabilizing mechanism due to the high-amplitude, periodic forcing. It is also interesting to note that the kinematic equation $\dot{\bar{\theta}} = \bar{q}$ is changed to $\dot{\bar{\theta}} = -2.90\bar{u} + 0.96\bar{q}$. This is because the time-periodic terms do not satisfy the condition $\int_0^T \int_0^t v(\tau)\,\mathrm{d}\tau\,\mathrm{d}t = 0$, where v is the zero-mean signal, see Bullo [35].

4.3. Full hovering dynamics: periodic orbit equilibrium

So far, we have investigated the flight dynamics of hovering insects and FWMAVs ignoring the zero-mean forcing term $g_1(t)$; the zero-mean part of the aerodynamic loads due to the flapping motion of the wing. Doing so yields a system with a fixed point, equation (8), that has been shown to be stabilized for the hawkmoth case due to the high-amplitude, periodic terms. The full dynamics (4) can be regarded as the system (8) subjected to a bounded, zero-mean, periodic forcing $g_1(t)$. A matter which, knowing that the system (8) is stable, may deceptively indicate stability of the periodic orbit produced by the external forcing $g_1(t)$. In this subsection, we determine the effect of $g_1(t)$ on the system dynamics.

Incorporating $g_1(t)$, the system cannot have a fixed point for all times and its equilibrium will rather be described by a periodic orbit. Knowing that, if the vehicle is balanced based on the average $f(\mathbf{0}) + \bar{g}_0 = \mathbf{0}$ (e.g., the cycle-averaged lift force is equal to the weight), then the origin is ensured to be a fixed point for the first-order averaged dynamics but not necessarily for the higher-order averaged dynamics. That is, the forcing term $g_1(t)$ may interact with the time-varying dynamics (represented in the

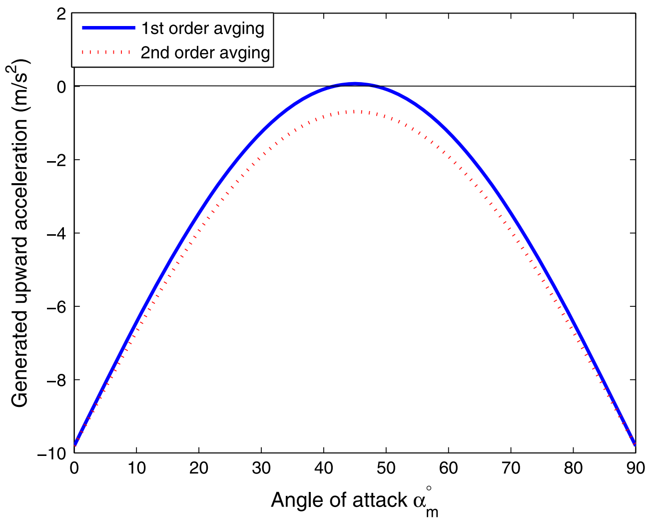

Figure 7. First-order and second-order averaging results for the variation of the generated upward acceleration with the angle of attack α_m using the triangular waveform and the documented $\Phi = 60.5°$ for the hawkmoth. Zero acceleration is required for trim.

parametric excitation $G_1(t)$), resulting in a constant drift in the higher-order averaged dynamics. This constant drift, in turn, changes the equilibrium state of the system. This phenomenon is referred to as direct/parametric interaction by Nayfeh and Mook [36]. This is an important note because if the system dynamics (4) is simulated using the flapping parameters that achieve balance/trim based on the average, the system will certainly deviate from the hovering condition. This behavior has nothing to do with the stability characteristics of hovering. It is just because the hovering flight condition is not truly balanced. This may explain why most of the previous studies concluded hovering instability; direct averaging falsely indicates instability and simulation deceptively shows deviation from hovering.

Using second-order averaging, the flapping parameters $\boldsymbol{P}$ are required to satisfy

$$\boldsymbol{\Lambda}_1\left(\boldsymbol{x}_{\text{eqm}};\, \boldsymbol{P}\right) + \boldsymbol{\Lambda}_2\left(\boldsymbol{x}_{\text{eqm}};\, \boldsymbol{P}\right) = \boldsymbol{0} \qquad (13)$$

to achieve trim/balance. If hovering equilibrium is desired, then, $\bar{u} = 0$, $\bar{w} = 0$, and $\bar{q} = 0$, while $\bar{\theta}$ can be any admissible value. That is, $\boldsymbol{x}_{\text{eqm}} = [0,\ 0,\ 0,\ \theta_{\text{eqm}}]^T$.

4.3.1. Symmetric flapping

Similar to the observed change in the kinematic equation $\dot{\theta} = q$ in the previous example, incorporating $\boldsymbol{g}_1(t)$ results in a constant drift in the corresponding second-order averaged equation. The fourth component of $\boldsymbol{\Lambda}_2$ is given by

$$\Lambda_{2,4}\left(\boldsymbol{x}_{\text{eqm}}\right) = 8\frac{K_{22}\Delta x\Phi\,\sin\,\Phi\,\sin\,\alpha_m}{TI_y}.$$

Thus, the only choice to eliminate this constant drift in the symmetric flapping case is to have $\Delta x = 0$; that is, the hinge line has to be aligned with the line passing through the wing's center of pressure. The drift in the pitching moment equation then becomes

$$\Lambda_{2,3}\left(\boldsymbol{x}_{\text{eqm}};\, \Delta x = 0\right) = -g\,\sin\,\theta_{\text{eqm}} \times \frac{K_{21}\,\sin\,2\alpha_m\left(\sin\,2\Phi - 2\,\cos\,2\Phi\right)}{4\Phi I_y}$$

which is eliminated by choosing $\theta_{\text{eqm}} = 0$. Now, we are left with two trim equations to be satisfied

$$\Lambda_{2,1}\left(\boldsymbol{0};\, \Delta x = 0,\, \Phi,\, \alpha_m\right) = 0,$$
$$\Lambda_{1,2}\left(\boldsymbol{0};\, \Delta x = 0,\, \Phi,\, \alpha_m\right) + \Lambda_{2,2}\left(\boldsymbol{0};\, \Delta x = 0,\, \Phi,\, \alpha_m\right) = 0. \qquad (14)$$

These are two nonlinear algebraic equations in the flapping amplitude Φ and the angle of attack α_m. For the hawkmoth case, one feasible solution to this set of equations is

$$\Phi = 83.05°, \qquad \alpha_m = 18.35°.$$

Many researchers, including the authors, have used the intuitive, ubiquitous balancing methodology based on direct averaging, either for aerodynamic optimization (minimum power or maximum thrust with cycle-averaged lift equal to the weight) [40–44] or flight dynamics and control analyzes [3, 4, 6–9, 15, 27, 30]. However, the above result shows that such a methodology is not sufficient to ensure trim/balance. That is, symmetric flapping does not ensure balance in the forward direction; a cycle-averaged lift equal to the weight does not ensure balance in the vertical direction; and aligning the hinge line with the vehicle's center of gravity is not enough to achieve pitch trim. In particular, figure 7 shows the first-order and second-order averaging results for the variation of the generated upward acceleration with the angle of attack α_m using the triangular waveform and the documented $\Phi = 60.5°$ for the hawkmoth. Figure 7 shows that direct averaging overestimates the generated lift force. That is, the oscillatory motion of the body due to the periodic forcing leads to a decrease in the generated lift force, which is consistent with the result of Wu *et al* [38]. This is because the oscillatory motion of the body induces a negative component to the velocity of the wing relative to the still air. As such, the FWMAV/insect has to flap so as to produce cycle-averaged lift (due to flapping) that is more than its weight. It should be noted that the total cycle-averaged lift (due to flapping and due to body motion), however, equals the weight at balance. Because of their potential importance, we provide in equations (15), (16) a general representation for the trim equations (14) to be used in the future aerodynamic and dynamic analyzes.

$$\begin{aligned}\boldsymbol{\Lambda}_{2,1}(\mathbf{0}) = \frac{1}{2T}\int_0^T \Bigg[\frac{1}{m}\Bigg(&X_u(t)\int_0^t X_0(\tau)\mathrm{d}\tau \\ &- X_0(t)\int_0^t X_u(\tau)\mathrm{d}\tau \\ &+ X_w(t)\int_0^t Z_0(\tau)\mathrm{d}\tau - Z_0(t) \\ &\times \int_0^t X_w(\tau)\mathrm{d}\tau\Bigg) + \frac{1}{I_y}\Big(X_q(t) \\ &\times \int_0^t M_0(\tau)\mathrm{d}\tau - M_0(t) \\ &\times \int_0^t X_q(\tau)\mathrm{d}\tau\Big)\Bigg]\mathrm{d}t,\end{aligned} \tag{15}$$

$$\begin{aligned}\boldsymbol{\Lambda}_{1,2}(\mathbf{0}) + \boldsymbol{\Lambda}_{2,2}(\mathbf{0}) = \frac{1}{2T}\int_0^T \Bigg[\frac{1}{m} \\ \times \Bigg(Z_u(t)\int_0^t X_0(\tau)\mathrm{d}\tau - X_0(t) \\ \times \int_0^t Z_u(\tau)\mathrm{d}\tau + Z_w(t) \\ \times \int_0^t Z_0(\tau)\mathrm{d}\tau - Z_0(t) \\ \times \int_0^t Z_w(\tau)\mathrm{d}\tau\Bigg) + \frac{1}{I_y}\Big(Z_q(t) \\ \times \int_0^t M_0(\tau)\mathrm{d}\tau - M_0(t)\int_0^t Z_q(\tau)\mathrm{d}\tau\Big)\Bigg]\mathrm{d}t \\ + \underbrace{g + \frac{1}{mT}\int_0^T Z_0(t)\mathrm{d}t}_{\text{1st order contribution}}.\end{aligned} \tag{16}$$

To appreciate the amplitude of the periodic forcing that hovering insects and FWMAVs experience, we note that the term $\frac{1}{I_y}M_0(t)$ has an amplitude of about 2700 rad s^{-2} in the hawkmoth case. It should also be noted that the constant drift (shift of the equilibrium) becomes more considerable for light vehicles flapping at low frequencies; that is, it is inversely proportional with the mass, moment of inertia, and flapping frequency.

Although the functional form of the matrix representing the linearized, second-order averaged dynamics $[D(\boldsymbol{\Lambda}_1 + \boldsymbol{\Lambda}_2)(\mathbf{0})]$ is exactly the same as that of the previous example (nonlinear flight dynamics, omitting periodic forcing), evaluating it at the new flapping parameters that achieve trim ($\Phi = 83.05°$, $\alpha_m = 18.35°$, and $\Delta x = 0$) yields an unstable fixed point with the following eigenvalues for the hawkmoth case:

$$3.64, \quad -5.16, \quad -28.02, \quad -6.49.$$

In addition, these flapping parameters result in another fixed point at

$$\bar{x} = \left[1.45 \text{ m s}^{-1}, \quad -3.03 \text{ m s}^{-1}, \quad 0.00, \quad -180°\right]^T$$

which corresponds to a vertical descent with a rate of 3.03 m s^{-1} and a backward motion at a speed of 1.45 m s^{-1} at a pitching angle of $-180°$. The eigenvalues of the matrix representing the linearization of the second-order averaged dynamics about this fixed point are

$$-2.81 \pm 3.03\mathrm{i}, \quad -23.93, \quad -6.48$$

which indicates stability of the vertical descent equilibrium. This analysis shows that any perturbation from the hovering equilibrium will lead to pitching down while descending and moving backward until the insect FWMAV reaches a stable upside-down descending equilibrium while moving backward. Figure 8 shows simulation of the system (4) using the new trim parameters supporting the above analysis.

4.3.2. Asymmetric flapping

Using symmetric flapping, we could not achieve balance at the documented Φ for the hawkmoth ($\Phi = 60.5°$ [45]). To obtain stability results that are more representative for the hovering hawkmoth, we use asymmetric flapping of the form

$$\varphi(t) = \begin{cases} \phi_0 + \dfrac{4\Phi}{T}\left(t - \dfrac{T}{4}\right), & 0 \leqslant t < \dfrac{T}{2} \\ \phi_0 - \dfrac{4\Phi}{T}\left(t - \dfrac{3T}{4}\right), & \dfrac{T}{2} \leqslant t < T \end{cases} \quad \text{and}$$

$$\eta(t) = \begin{cases} \alpha_d, & 0 \leqslant t < \dfrac{T}{2}, \\ \pi - \alpha_u, & \dfrac{T}{2} \leqslant t < T, \end{cases} \tag{17}$$

where ϕ_0 is an offset angle to create asymmetry for the triangular waveform of $\varphi(t)$ and α_d and α_u are the angles of attack during the downstroke and upstroke, respectively. In addition, we use the documented x_h of the hovering hawkmoth ($x_h = 0.22R$ [15]). Then, we seek the flapping parameters $\alpha_d, \alpha_u, \phi_0$, and Δx and the operating θ_{eqm} to ensure trim of the second-order averaged dynamics at hover; that is, to satisfy equation (13). Using least squares analysis, we obtain

$$\alpha_d = 44.93°, \quad \alpha_u = 44.93°, \quad \phi_0 = -38.1569°,$$
$$\Delta x = 0.42, \quad \theta_{\text{eqm}} = 2.48°.$$

Linearizing the second-order averaged dynamics about the ensured fixed point, the eigenvalues of the system matrix are

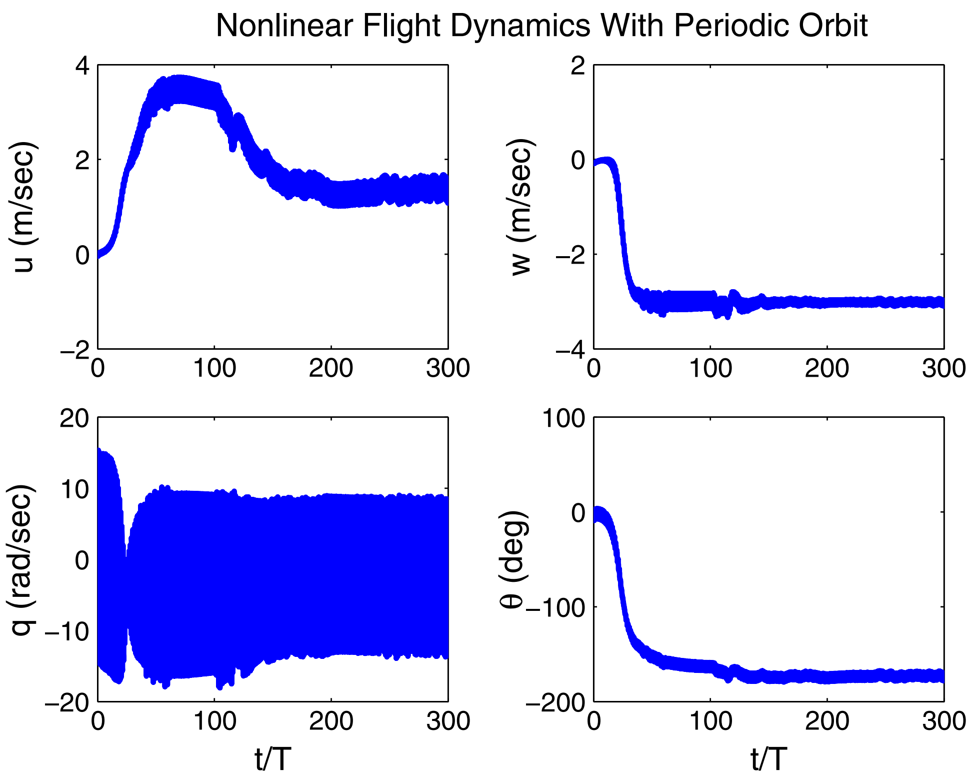

Figure 8. Simulation of the full nonlinear flight dynamics with periodic orbit for the hawkmoth case.

$$2.73, \quad -4.80 \pm 4.57i, \quad -2.77$$

which indicates instability of the hovering hawkmoth.

In summary, the hovering equilibrium is indeed unstable, but for reasons that are more subtle than the earlier analysis has suggested. Moreover, the adopted methodology reveals some interesting facts about the dynamics of flapping flight. Specifically, the high-amplitude, periodic forcing may lead to stabilizing actions as shown in the case of the dynamics with fixed point (omitting the periodic external forcing). It may also lead to a change in the equilibrium state, which dictates that the FWMAV/insect has to flap more to keep balance.

5. On the applicability of direct averaging

In this section, we consider the hovering dynamics of four other insects; namely, the cranefly, bumblebee, dragonfly, and hoverfly. These insects, along with the hawkmoth, cover a wide range of operating conditions. Their morphological parameters are given in appendix A. The objective is to determine an estimate for the region of applicability of direct averaging in analyzing the flight dynamics of hovering insects and FWMAVs. This is performed by comparing the stability characteristics using direct averaging and the second-order averaging for all of the insects. We use the ratio of the flapping frequency to the natural frequency of body dynamics as the basis of comparison. It should be noted that such comparison will not be appropriate if it is performed using the full flight dynamics (with periodic orbit), because second-order averaging requires different flapping parameters to achieve balance than those required by direct averaging, as shown in section 4.3. Thus, to perform the comparison having the same equilibrium (using the same set of trim flapping parameters), the flight dynamics with fixed point is considered; i.e., equation (8).

Table 1 shows the ratios of flapping frequency to the body natural frequency for the five insects, and the eigenvalues revealing the stability of the system (8) using first-order and second-order averaging. It is noteworthy to mention that the ratio $\frac{2\pi f}{\omega_n}$ is not monotonically increasing with f as the increase in the flapping frequency f may be associated with a larger increase in the body-motion natural frequency ω_n, as shown in the hoverfly case in comparison to the dragonfly. We note that the body mass of the hoverfly is considerably smaller than that of the dragonfly as shown in table A1.

Table 1 shows that the high-frequency, high-amplitude, periodic forcing does not considerably impact the stability characteristics of hovering insects and FWMAVs for large $\frac{2\pi f}{\omega_n}$ ratios (above 100). That is, direct averaging is capable of capturing the true stability characteristics over this range. This result is consistent with that obtained by the MMS [19]. It should be noted that all of the insects exhibit creation of stabilizing pitching stiffness due to the high-frequency, high-amplitude,

Table 1. The eigenvalues revealing the stability of the system (8) using first-order and second-averaging for the five insects along with the ratio of the flapping frequency to the natural frequency ω_n of the flight dynamics. $\overline{C_{M\theta}}$ is the pitch stiffness coefficient that is induced by the high-frequency, high-amplitude, periodic terms.

Insect	$\frac{2\pi f}{\omega_n}$	λ_{1st}	λ_{2nd}	$\overline{C_{M\theta}}$
Hawkmoth	28.78	[−11.89, −3.30, 0.19 ± 5.74i]	[−10.40, −3.09, −0.66 ± 3.72i]	−0.0302
Cranefly	50.62	[−47.71, −17.31, −1.13 ± 5.53i]	[−45.76, −16.26, −13.16, 7.90]	−0.0661
Bumblebee	144.46	[−11.63, −4.39, 1.58 ± 6.55i]	[−11.26, −4.37, 1.38 ± 6.17i]	−0.0033
Dragonfly	145.50	[−13.11, −7.03, 1.34 ± 6.65i]	[−12.56, −6.98, 1.04 ± 5.99i]	−0.0038
Hoverfly	113.98	[−14.01, −7.27, 2.13 ± 8.56i]	[−13.37, −7.24, 1.79 ± 7.92i]	−0.0083

Table A1. The morphological parameters for the five studied insects.

Insect	f (Hz)	$\Phi°$	S (mm^2)	R(mm)	$\bar{c}$ (mm)	$\hat{r}_1$	$\hat{r}_2$	m (mg)	I_y (mg. cm^2)
Hawkmoth	26.3	60.5	947.8	51.9	18.3	0.440	0.525	1648	2080
Cranefly	45.5	61.5	30.2	12.7	2.38	0.554	0.601	11.4	0.95
Bumblebee	155	58.0	54.9	13.2	4.02	0.490	0.550	175	21.3
Dragonfly	157	54.5	36.9	11.4	3.19	0.481	0.543	68.4	7.0
Hoverfly	160	45.0	20.5	9.3	2.20	0.516	0.570	27.3	1.84

periodic forcing. However, table 1 shows that there are cases where this stabilizing effect is not strong enough (the cases of $\frac{2\pi f}{\omega_n} > 100$), cases where the net result is a destabilizing effect rather (cranefly), and cases where the induced pitch stiffness is enough to stabilize the system dynamics. Unlike all of the other insects, the hovering dynamics of the cranefly exihibits a considerable increase in the speed stability (M_u), which is a harmful effect as shown in [27]. As such, although the cranefly hovering dynamics exhibits the largest induced pitch stiffness, the net effect of the high-frequency, high-amplitude, periodic forcing is destabilizing.

6. Conclusion

The longitudinal flight dynamics of FWMAVs and insects is considered. The results show that direct averaging is not sufficient to assess the hovering stability of the relatively low flapping frequency systems. Typically, direct averaging is applicable for flapping-to-natural frequency ratios above 100. On the other hand, the complication of the Floquet theorem approach dictates numerical implementation of the theorem and precludes any analytical treatment of the problem. In addition, careless choices of the integrator and its time-step may lead to false conclusions about the stability of such systems. The results also show that higher-order averaging is suitable to analyze the flight dynamics of hovering insects and FWMAVs as it overcomes the issues with the other approaches (direct averaging and Floquet theorem). Adopting this methodology, we show that the high-frequency, high-amplitude, periodic forcing associated with flapping cannot be neglected as it induces stabilizing pitch stiffness for the studied five insects. It may also lead to a change in the equilibrium state. This refutes the previous common intuition about balancing a hovering vehicle. That is, symmetric flapping does not ensure zero cycle-averaged forward thrust force, a cycle-averaged lift equal to the weight does not ensure balance in the vertical direction, and aligning the hinge line with the vehicle's center of gravity is not enough to achieve self pitch trim. In contrast, the FWMAV/insect has to provide an average lift due to flapping that is more than its weight to keep balance.

Acknowledgment

The authors acknowledge the support of NSF Grant CMMI-1435484.

Appendix A. Morphological parameters

Table A1 shows the morphological parameters of the five studied insects as given in [15] and [45].

The moments of the wing chord distribution $\hat{r}_1$ and $\hat{r}_2$ are defined as

$$I_{k1} = 2\int_0^R r^k c(r)\, dr = 2SR^k \hat{r}_k^k.$$

As for the wing planform, the method of moments used by Ellington [45] is adopted to obtain a chord-distribution for the insect that matches the documented first two moments $\hat{r}_1$ and $\hat{r}_2$, that is,

$$c(r) = \frac{\bar{c}}{\beta}\left(\frac{r}{R}\right)^{\alpha-1}\left(1-\frac{r}{R}\right)^{\gamma-1},$$

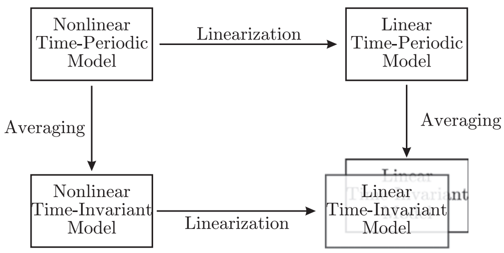

Figure B1. Averaging and linearization.

where

$$\alpha = \hat{r}_1\left[\frac{\hat{r}_1\left(1-\hat{r}_1\right)}{\hat{r}_2^2-\hat{r}_1^2}-1\right],$$

$$\gamma = \left(1-\hat{r}_1\right)\left[\frac{\hat{r}_1\left(1-\hat{r}_1\right)}{\hat{r}_2^2-\hat{r}_1^2}-1\right]$$

$$\text{and}\quad \beta = \int_0^1 \hat{r}^{\alpha-1}\left(1-\hat{r}\right)^{\gamma-1}\,\mathrm{d}\hat{r}.$$

Appendix B. On the commutativity of linearization and averaging

Consider the NLTP system

$$\dot{x} = \epsilon f(x, t), \tag{B.1}$$

where $\epsilon \ll 1$ and the vector field f is continuously differentiable in its first argument and T-periodic in its second argument. The first-order averaged approximation of the system (B.1) is

$$\dot{\bar{x}} = \epsilon \bar{f}\left(\bar{x}\right), \tag{B.2}$$

where

$$\bar{f}\left(\bar{x}\right) = \frac{1}{T}\int_0^T f\left(\bar{x}, t\right)\mathrm{d}t. \tag{B.3}$$

The system (B.2) is a NLTI system. Suppose that (B.2) possesses a fixed point p_0. Linearizing equation (B.2) about this equilibrium results in the LTI system

$$\boldsymbol{\delta}\dot{\bar{x}} = \epsilon \bar{F}\boldsymbol{\delta}\bar{x}, \tag{B.4}$$

where

$$\bar{F} = \left.\frac{\partial \bar{f}(x)}{\partial x}\right|_{x=p_0} \tag{B.5}$$

is a constant matrix. According to the averaging theorem [46], if p_0 is a hyperbolic equilibrium point of (B.2), then there exists $\epsilon_0 > 0$ such that for all $0 < \epsilon \leqslant \epsilon_0$, the system (B.1) possesses a unique hyperbolic periodic orbit $p(t) = p_0 + O(\epsilon)$ of the same stability type as p_0.

Linearizing the system (B.1) about its periodic orbit $p(t)$ results in a LTP system

$$\boldsymbol{\delta}\dot{z} = \epsilon G(t)\boldsymbol{\delta}z, \tag{B.6}$$

where

$$G(t) = \left.\frac{\partial f(z, t)}{\partial z}\right|_{z=p(t)}.$$

The first-order averaged form of equation (B.6) is

$$\boldsymbol{\delta}\dot{\bar{z}} = \epsilon \bar{G}\boldsymbol{\delta}\bar{z}, \tag{B.7}$$

where

$$\bar{G} = \frac{1}{T}\int_0^T G(t)\,\mathrm{d}t. \tag{B.8}$$

In summary, one may average the NLTP system (B.1) and then linearize about the fixed point p_0 to obtain the LTI system (B.4). *Or* one may linearize the NLTP system (B.1) around the periodic orbit $p(t)$ and then average to obtain the LTI system (B.7). However, the systems (B.4) and (B.7) that result from these two approximation sequences are not identical, as depicted in figure B1 .

To appreciate the disparity between the systems (B.4) and (B.7), we consider the error that accrues during first-order averaging and linearization. Using the Taylor series expansion of $f(x, t)$ around p_0, and assuming that $\| x(t) - p_0 \|$ is sufficiently small, one finds that

$$\begin{aligned}
\bar{G} &= \frac{1}{T}\int_0^T \left(\left.\frac{\partial f(x, t)}{\partial x}\right|_{x=p_0} + O(\epsilon)\right)\mathrm{d}t \\
&= \frac{1}{T}\int_0^T \left.\frac{\partial f(x, t)}{\partial x}\right|_{x=p_0}\mathrm{d}t + O(\epsilon) \\
&= \left[\frac{\partial}{\partial x}\left(\frac{1}{T}\int_0^T f(x, t)\,\mathrm{d}t\right)\right]_{x=p_0} + O(\epsilon) \\
&= \left.\frac{\partial \bar{f}(x)}{\partial x}\right|_{x=p_0} + O(\epsilon) \\
&= \bar{F} + O(\epsilon).
\end{aligned} \tag{B.9}$$

Thus, if $\boldsymbol{\delta}\bar{x}(t)$ and $\boldsymbol{\delta}\bar{z}(t)$ are solutions of (B.4) and (B.7) starting from initial conditions $\boldsymbol{\delta}\bar{x}_0$ and $\boldsymbol{\delta}\bar{z}_0$, respectively with $\|\boldsymbol{\delta}\bar{x}_0 - \boldsymbol{\delta}\bar{z}_0\| = O(\epsilon)$, then $\|\boldsymbol{\delta}\bar{x}(t) - \boldsymbol{\delta}\bar{z}(t)\| = O(\epsilon)$ on a time scale $\frac{1}{\epsilon}$. Moreover if the hyperbolic equilibrium point p_0 of (B.2), and therefore the hyperbolic periodic orbit $p(t)$ of (B.1), is stable, then the LTI systems (B.4) and (B.7) are stable and $\|\boldsymbol{\delta}\bar{x}(t) - \bar{\delta z}(t)\| = O(\epsilon)$ for $t \in [0, \infty)$. For proof of a similar case, see [46].

Finally, the reader may not find the relation between the above non-commutativity property and the work performed in this paper clear enough. This is because the solution considered here, equilibrium solution of the system (8), is not a periodic orbit but a fixed point for a NLTP system. In such a case, the commutativity between linearization and averaging holds. Therefore, we provide this appendix here to warn the reader about the invalidity of such a a commutativity, in general.

References

[1] Thomas A L R and Taylor G K 2001 *J. Theor. Biol.* **212** 399–424
[2] Khan Z A and Agrawal S K 2007 *IEEE American Control Conf.* pp 5284–9
[3] Sun M and Xiong Y 2005 *J. Exp. Biol.* **208** 447–59
[4] Xiong Y and Sun M 2008 *Acta Mech. Sin.* **24** 25–36
[5] Dietl J M and Garcia E 2008 *J. Guid. Control Dyn.* **31** 1157–62
[6] Schenato L, Campolo D and Sastry S S 2003 *42nd IEEE Conf. on Decision and Control* **vol 6** pp 6441–7
[7] Deng X, Schenato L, Wu W C and Sastry S S 2006 *IEEE Trans. Robot.* **22** 789–803
[8] Doman D B, Oppenheimer M W and Sigthorsson D O 2010 *J. Guid. Control Dyn.* **33** 724–39
[9] Oppenheimer M W, Doman D B and Sigthorsson D O 2011 *J. Guid. Control Dyn.* **34** 204–17
[10] Taha H E, Hajj M R and Nayfeh A H 2013 Aero-Dynamic interaction and longitudinal stability of hovering MAVs/insects *Proc. 54th (AIAA/ASME/ASCE/AHS/ACS) Structures, Structural Dynamics, and Materials Conference (Boston MA, Apr 2013)* 2013-1707
[11] Taha H E, Hajj M R and Nayfeh A H 2012 *Nonlinear Dyn.* **70** 907–39
[12] Sun M 2014 *Rev. Mod. Phys.* **86** 615
[13] Taylor G K and Thomas A L R 2002 *J. Theor. Biol.* **214**
[14] Taylor G K and Thomas A L R 2003 *J. Theor. Biol.* **206** 2803–29
[15] Sun M, Wang J and Xiong Y 2007 *Acta Mech. Sin.* **23** 231–46
[16] Bierling T and Patil M 2009 *Int. Forum on Aeroelasticity and Structural Dynamics* pp 2–5
[17] Su W and Cesnik C E S 2011 Flight dynamic stability of a flapping wing micro air vehicle in hover *Proc. 52nd AIAA/ASME/ASCE/AHS/ASC Structures, Structural Dynamics, and Materials Conference* (Denver CO April 2011) AIAA-2011-2009
[18] Alexander D E and Vogel S 2004 *Nature's Flyers: Birds, Insects, and the Biomechanics of Flight* (Baltimore, MD: John Hopkins University Press)
[19] Taha H E, Nayfeh A H and Hajj M R 2014 *Nonlinear Dyn.* **78** 2399–2408
[20] Nayfeh A H 1973 *Perturbation Methods* (New York: Wiley)
[21] Nayfeh A H 1981 *Introduction to Perturbation Techniques* (New York: Wiley)
[22] Sarychev A 2001 *Nonlinear Control in the Year 2000* (*Lecture Notes in Control and Information Sciences* vol 2) (Berlin: Springer)
[23] Vela P A 2003 Averaging and control of nonlinear systems (with application to biomimetic locomotion) *PhD Thesis* California Institute of Technology Pasadena, CA
[24] Agrachev A A and Gamkrelidze R V 1979 *Math. USSR: Sb.* **35** 727–85
[25] Nelson R C 1989 *Flight Stability and Automatic Control* (New York: McGraw-Hill)
[26] Taha H E, Hajj M R and Nayfeh A H 2013 *J. Aircr.* **50** 610–4
[27] Taha H E, Hajj M R and Nayfeh A H 2014 *J. Guid. Control Dyn.* **37** 970–8
[28] Taha H E, Hajj M R and Beran P S 2013 Unsteady nonlinear aerodynamics of hovering MAVs/insects *Proc. 51st AIAA Aerospace Sciences Meeting* (Grapevine TX, Jan 2013) 2013-0504
[29] Taha H E, Hajj M R and Beran P S 2014 *Aerosp. Sci. Technol.* **34** 1–11
[30] Cheng B and Deng X 2011 *IEEE Trans. Robot.* **27** 849–64
[31] Khalil H K 2002 *Nonlinear Systems* 3rd edn (Englewood Cliffs, NJ: Prentice-Hall)
[32] Schenato L 2003 Analysis and control of flapping flight: from biological to robotic insects *PhD Thesis* University of California, Berkeley
[33] Orlowski C T and Girard A R 2011 *AIAA J.* **49** 969–81
[34] Orlowski C T and Girard A R 2011 Modeling and simulation of nonlinear dynamics of flapping wing micro air vehicles *AIAA J.* **49** 969–81
[35] Bullo F 2002 *SIAM J. Control Optim.* **41** 542–62
[36] Nayfeh A H and Mook D T 1979 *Nonlinear Oscillations* (New York: Wiley)
[37] Nayfeh A H and Balachandran B 1995 *Applied Nonlinear Dynamics* (New York: Wiley)
[38] Wu J H, Zhang Y L and Sun M 2009 *J. Exp. Biol.* **212** 3313–29
[39] Ogata K 1987 *Discrete-Time Control Systems* vol 1 (Englewood Cliffs, NJ: Prentice-Hall)
[40] Berman G J and Wang Z J 2007 *J. Fluid Mech.* **582** 153–68
[41] Kurdi M, Stanford B and Beran P 2010 Kinematic optimization of insect flight for minimum mechanical power *Proc. 48th AIAA Aerospace Sciences Meeting* (Orlando FL, Jan 2010) 2010-1420
[42] Ghommem M, Hajj M R, Mook D T, Stanford B K, Beran P S, Snyder R D and Watson L T 2012 *J. Fluids Struct.* **33** 210–28
[43] Stanford B K, Beran P S, Snyder R and Patil M 2012 *53rd AIAA/ASME/ASCE/AHS/ASC Structures, Structural Dynamics and Materials Conf. (Honolulu, Hawaii)* AIAA 2012-1638
[44] Taha H E, Hajj M R, Roman A H and Nayfeh A H 2014 *J. Guid. Control Dyn.* **37** 167–372
[45] Ellington C P 1984 *Phil. Trans. R. Soc.* B **305** 17–40
[46] Guckenheimer J and Holmes P 1983 *Nonlinear Oscillations, Dynamical Systems, and Bifurcations of Vector Fields* (New York: Academic)